Comparison of Pseudo-Spectral Algorithms for Field-Theoretic Simulations of Polymers

Debra J. Audus,[†,‡] Kris T. Delaney,[†] Hector D. Ceniceros,[¶] and Glenn H. Fredrickson[*,†,‡,§]

Materials Research Laboratory, University of California, Santa Barbara, CA, 93106, Department of Chemical Engineering, University of California, Santa Barbara, CA, 93106, Department of Mathematics, University of California, Santa Barbara, CA, 93106, and Department of Materials, University of California, Santa Barbara, CA, 93106

E-mail: ghf@mrl.ucsb.edu

Abstract

We compare three pseudo-spectral algorithms for mean-field polymer self-consistent field theory (SCFT) simulations and beyond mean-field field-theoretic simulations (FTS) using the complex Langevin (CL) sampling technique. In agreement with a study by Stasiak and Matsen, we find that for SCFT the fourth-order algorithm developed by Ranjan, Qin and Morse usually outperforms the other pseudo-spectral algorithms. In contrast, for CL simulations we find that the second-order algorithm adapted to SCFT by Rasmussen and coworkers often outperforms the fourth-order methods not only in computational speed but also, surprisingly, in accuracy at a fixed contour resolution. This suggests an intricate coupling between pseudo-spectral

[*]To whom correspondence should be addressed
[†]Materials Research Laboratory, University of California, Santa Barbara, CA, 93106
[‡]Department of Chemical Engineering, University of California, Santa Barbara, CA, 93106
[¶]Department of Mathematics, University of California, Santa Barbara, CA, 93106
[§]Department of Materials, University of California, Santa Barbara, CA, 93106

schemes for chain contour integration and pseudo-time stepping methods in CL simulations. Finally, the nominal stability of the algorithms is examined for the case of homogeneous fields.

Introduction

In the study of self-assembling polymeric materials, self-consistent field theory (SCFT) simulations have proven to be a versatile and powerful tool.[1–3] More recently, field-theoretic simulations (FTS) using a complex Langevin (CL) sampling method have been introduced to study systems for which the mean-field approximation inherent in SCFT fails, such as block copolymer melts near the order-disorder boundary or polymer solutions.[4,5] However, identifying an efficient and stable numerical method for solving the computationally costly modified diffusion equation (MDE) in both SCFT and CL can prove challenging. Many approaches have been developed for solving the MDE, the two most popular being the spectral method[6] and the pseudo-spectral[7] method. The spectral method is prohibitively expensive unless a small number of basis functions is used. In practice, for systems with long-range order a constraining symmetry class is usually imposed on a unit cell, reducing the computational effort but requiring knowledge of the microphase structure of interest. The pseudo-spectral method, in contrast, does not require *a priori* knowledge of the structure of the phase and thus is very useful for problems where the structure is unknown, such as systems with new polymer architectures or under confinement. Pseudo-spectral algorithms are also ideally suited to systems with only short-ranged order, especially those with composition fluctuations; they are the only methods successfully applied to date in CL simulations.

In both pseudo-spectral SCFT and CL, the most computationally demanding step is finding the solution of the MDE

$$\frac{\partial q(\mathbf{r},s;[w])}{\partial s} = \nabla^2 q(\mathbf{r},s;[w]) - w(\mathbf{r},s)q(\mathbf{r},s;[w]), \tag{1}$$

which involves solving for a propagator $q(\mathbf{r},s;[w])$ that is a function of both space ($\mathbf{r}$) and a contour variable parameterizing the polymer backbone (s). $w(\mathbf{r},s)$ is a specified auxiliary field that depends

on the species of the polymer segment at s. Physically, the propagator represents the probability of finding the polymer end segment associated with the contour point s at a given spatial point $\mathbf{r}$ and is a central quantity in all field-based polymer simulations. For untethered polymers, the MDE is subject to an initial condition of $q(\mathbf{r}, s = 0; [w]) = 1$, implying that a polymer of zero length is unbiased by the imposed w field.

Three pseudo-spectral algorithms have been adopted for solving the MDE in the context of polymer simulations. In 2002, Rasmussen and Kalosakas[7] and Tzeremes *et al.*[8] introduced a second-order method (RK2) that is an application of Strang splitting[9] and requires one forward and one backward fast Fourier transform (FFT) on $\mathbf{r}$ per discrete contour step Δs. In 2008, Ranjan, Qin and Morse[10] extended RK2 to fourth-order accuracy using Richardson extrapolation. The resulting method (RQM4) requires three forward and three backward FFTs on $\mathbf{r}$ per discrete contour step. In 2006, Cochran, García-Cervera and Fredrickson[11,12] introduced a fourth-order algorithm (CGF4) that uses operator splitting and treats the Laplacian operator implicitly with a backwards differentiation formula and the field operator explicitly with a Adams-Bashford formula. This algorithm like RK2 only requires one forward and one backward FFT on $\mathbf{r}$ per discrete contour step. Note that our quoted order of accuracy for each method refers to the *global* error in Δs. While these algorithms are most simply applied to systems in bulk with periodic boundary conditions, they can be easily extended via discrete sine or cosine transforms to confined polymer films subject to either Neumann or Dirichlet boundary conditions.[2,13]

Since the MDE is the most expensive step in both SCFT and CL, a proper choice of algorithm is critical to conducting efficient calculations. Here, we compare the performance of the three algorithms mentioned above for a variety of contour and spatial resolutions in the context of both static fields and full simulations using the canonical system of a diblock copolymer melt. Previously, Stasiak and Matsen[14] studied the error in the mean-field free energy as a function of both contour and spatial resolution for each method in SCFT simulations and presented timing data at various resolutions. We revisit this comparison providing timing data for a wider range of contour and spatial resolutions and discuss why the metric for convergence fails to reach a specified

tolerance for some SCFT simulations using the CGF4 algorithm; this lack of convergence was previously observed.[14] Additionally, we present the first study comparing the three algorithms for the increasingly popular technique of CL, where spatially non-smooth and complex-valued field configurations enter the MDE. Due to the comprehensive nature of the previous study[14] for SCFT and the lack of guidance for CL, we focus our efforts on algorithm choice in the context of CL and compare and contrast these results to the analogous results for SCFT. We also investigate the stability of the three algorithms in the special case of homogeneous fields, for which the stability can be determined analytically.

We first discuss the canonical diblock copolymer system, its governing equations and numerical algorithms in the Methods section. Next, the results of our study on the performance of the algorithms in the context of SCFT and CL are presented in the Results and Discussion section; the stability analysis can also be found in this section. Finally, we summarize our results and provide suggestions for algorithm choice for SCFT and CL in the Conclusions section.

Methods

Diblock copolymer melt

The field-theoretic canonical partition function for a system of n incompressible AB diblock copolymers with length N and a volume fraction of A segments of f in a volume V can be written as

$$\mathscr{Z}_C(n,V,T) = \mathscr{Z}_0 \int \mathscr{D}w_+ \int \mathscr{D}w_- \exp(-H[w_+,w_-]) \tag{2}$$

where $\mathscr{Z}_0$ contains ideal terms and other constants, w_+ and w_- are fields, $\int \mathscr{D}w$ denotes a functional integral over domain supported real-valued fields, and H is the Hamiltonian (see Fredrickson[2] for a more complete discussion). This Hamiltonian can be expressed as

$$H[w_+,w_-] = C \int d\mathbf{r} \left(\frac{w_-^2(\mathbf{r})}{\chi N} - i w_+(\mathbf{r}) \right) - CV \ln Q[w] \tag{3}$$

where all lengths are scaled by the radius of gyration R_g. The interactions between the A and B segments are described by the Flory-Huggins parameter χ, and the polymer concentration C is defined as n/V. Since the volume is scaled by R_g^3, the parameter C is a dimensionless measure of the number of copolymers penetrating a particular polymer coil. The final term in the Hamiltonian, Q, is the single chain partition function, which enumerates the conformational states of a non-interacting polymer chain subject to an external potential, and can be computed from the propagator as

$$Q = \frac{1}{V}\int d\mathbf{r}\, q(\mathbf{r}, s=1; [w]). \tag{4}$$

with w defined as

$$w(\mathbf{r},s) \equiv \begin{cases} iw_+(\mathbf{r}) - w_-(\mathbf{r}) & s \leq f \\ iw_+(\mathbf{r}) + w_-(\mathbf{r}) & s > f \end{cases} \tag{5}$$

Given the governing equations, we consider the two simulation techniques of interest.

SCFT

In SCFT simulations, the mean-field approximation is invoked so that instead of sampling the path integrals in the canonical partition function (eq 2), a single “saddle point" configuration is assumed to dominate the canonical partition function. Consequently,

$$\mathscr{Z}_C(n,V,T) \propto \exp(-H[w_+^*, w_-^*]) \tag{6}$$

where $w_+^*(\mathbf{r})$ and $w_-^*(\mathbf{r})$ are the field values associated with the saddle point field configuration. The free energy F of the system can then be written as $H[w_+^*, w_-^*]$ to within an additive constant. To find the saddle point fields, the stationary state of the Hamiltonian is calculated for both w_- and w_+. Thus,

$$\left.\frac{\delta H[w_+, w_-]}{\delta w_\pm(\mathbf{r})}\right|_{w_\pm^*} = 0. \tag{7}$$

The relevant functional derivatives are

$$\frac{\delta H[w_+, w_-]}{\delta w_-(\mathbf{r})} = C\left(\frac{2w_-(\mathbf{r})}{\chi N} - \phi_A(\mathbf{r}) + \phi_B(\mathbf{r})\right), \tag{8}$$

$$\frac{\delta H[w_+, w_-]}{\delta w_+(\mathbf{r})} = iC\left(-1 + \phi_A(\mathbf{r}) + \phi_B(\mathbf{r})\right) \tag{9}$$

where the volume fractions ϕ_A and ϕ_B are

$$\phi_A(\mathbf{r}) = \frac{1}{Q}\int_0^f ds\, q(\mathbf{r}, s) q^\dagger(\mathbf{r}, 1-s), \tag{10}$$

$$\phi_B(\mathbf{r}) = \frac{1}{Q}\int_f^1 ds\, q(\mathbf{r}, s) q^\dagger(\mathbf{r}, 1-s) \tag{11}$$

and the backward propagator $q^\dagger$ satisfies

$$\frac{\partial q^\dagger(\mathbf{r}, s; [w])}{\partial s} = \nabla^2 q^\dagger(\mathbf{r}, s; [w]) - w(\mathbf{r}, 1-s) q^\dagger(\mathbf{r}, s; [w]) \tag{12}$$

with $q^\dagger(\mathbf{r}, s = 0) = 1$.

A convenient way to solve eq 7 is to employ a steepest descent technique, which results in the relaxation scheme

$$\frac{\partial w_\pm(\mathbf{r}, t)}{\partial t} = -\lambda_\pm \frac{\delta H[w_+, w_-]}{\delta w_\pm(\mathbf{r})} \tag{13}$$

where t is a fictitious time and $\lambda_\pm$ is a real, positive constant that can be chosen to improve numerical stability. When this equation reaches steady state, the mean-field equation (eq 7) is automatically satisfied. For the w_+ field, which is constrained to be purely imaginary, the steepest descent scheme becomes a steepest ascent scheme to the saddle point upon Wick rotation.

Of course, the mean-field approximation is not always valid. For the case of diblock copolymers, this assumption breaks down at low C or close to the order-disorder transition. In these regions of parameter space, other techniques must be used to accurately simulate the system.

Complex Langevin

The technique of CL, unlike SCFT, samples the full path integrals in the canonical partition function where thermal fluctuations are important and the saddle point is no longer valid. CL simulations involve integrating the following stochastic differential system

$$\frac{\partial w_{\pm}(\mathbf{r},t)}{\partial t} = -\lambda_{\pm}\frac{\delta H[w_+,w_-]}{\delta w_{\pm}(\mathbf{r})} + \eta_{\pm}(\mathbf{r},t) \tag{14}$$

for both fields where t and $\lambda_{\pm}$ have the same meanings as in eq 13 and $\eta_{\pm}$ is Gaussian white noise which obeys the following statistics

$$\langle \eta_{\pm}(\mathbf{r},t)\rangle = 0, \tag{15}$$

$$\langle \eta_{\pm}(\mathbf{r},t)\eta_{\pm}(\mathbf{r}',t')\rangle = 2,\lambda_{\pm}\delta(\mathbf{r}-\mathbf{r}')\delta(t-t'). \tag{16}$$

Note that in the absence of the noise term, eq 14 reverts to the steepest descent equation for SCFT (eq 13). Using CL, the average value of quantities of interest can be computed as

$$\langle G\rangle = \frac{\mathscr{Z}_0}{\mathscr{Z}_C}\int \mathscr{D}w_+ \int \mathscr{D}w_- \, G[w_+,w_-]\exp(-H[w_+,w_-]), \tag{17}$$

where G is the quantity of interest such the Hamiltonian. Unlike SCFT, the free energy cannot be computed directly but instead requires more advanced techniques such as thermodynamic integration.[15] A more complete discussion of the CL technique in the context of polymer simulations can be found elsewhere.[2,4,5]

Numerical Methods

For both SCFT simulations and CL simulations, the equations are discretized in space ($\mathbf{r}$), contour step (s), and pseudo-time (t) and are supplemented with boundary conditions. Since we are interested in bulk unit cell calculations, we have chosen periodic boundary conditions for our sim-

ulations. Two types of numerical schemes are required: one to solve the MDE (eq 1) and one to solve for the fields as a function of pseudo-time (eq 13 for SCFT and eq 14 for CL).

Modified Diffusion Equation

We are interested in the relative performance of three pseudo-spectral methods. For each of these methods, the propagator at the next contour step ($q_{n+1} = q(\mathbf{r}, s_n + \Delta s)$) is solved using the propagator at the current step ($q_n = q(\mathbf{r}, s_n)$) and, in the case of CGF4, previous contour steps. We consider first the second order method (RK2) proposed by Rasmussen and Kalosakas[7] and Tzeremes *et al.*[8]

$$q_{n+1} = \mathscr{R}_{\Delta s} q_n \tag{18}$$

where

$$\mathscr{R}_{\Delta s} = \exp(-w(\mathbf{r})\Delta s/2)\exp(\Delta s \nabla^2)\exp(-w(\mathbf{r})\Delta s/2) \tag{19}$$

This method is an application of Strang splitting.[9] The symmetric breakup of the w operator makes RK2 ensures that odd powers of the global error are eliminated. The solution of the algorithm is a three step process per contour point. First, q_n is multiplied by $\exp(-w(\mathbf{r})\Delta s/2)$ and Fourier transformed. It is then multiplied by the Fourier representation of $\exp(\Delta s \nabla^2)$ and backward Fourier transformed. Finally, it is multiplied by $\exp(-w(\mathbf{r})\Delta s/2)$, yielding q_{n+1} and requires only a single FFT pair per discrete contour step. The computation effort of these limiting FFTs, scales as $M \log M$ per contour step where M is the total number spatial grid points.

The second method, RQM4, developed by Ranjan, Qin and Morse[10] is an extension of RK2 to fourth-order using Richardson extrapolation. This scheme can be written as

$$q_{n+1} = \left(\frac{4}{3}\mathscr{R}^2_{\Delta s/2} - \frac{1}{3}\mathscr{R}_{\Delta s} \right) q_n \tag{20}$$

and requires three FFT pairs per contour step rather than one as in RK2. Richardson extrapolation yields a fourth-order accurate method as the truncation error for eq 18 contains only even powers

of Δs.

The final algorithm of interest, CGF4, developed by Cochran, García-Cervera and Fredrickson[11,12] treats the Laplacian operator implicitly with a backwards differentiation formula and the field operator explicitly with an Adams-Bashford formula. This results in

$$q_{n+1} = \frac{1}{\frac{25}{12} - \Delta s \nabla^2} \left(4q_n - 3q_{n-1} + \frac{4}{3}q_{n-2} - \frac{1}{4}q_{n-3} + \Delta s w \left(-4q_n + 6q_{n-1} - 4q_{n-2} + q_{n-3}\right) \right) \tag{21}$$

assuming a fixed Δs and w across all of the contour steps, i.e. q_j for $n-3 \leq j \leq n+1$. This algorithm only requires one FFT pair per discrete contour step, but as a multi-step scheme, it needs initialization with another fourth-order method. This initialization is required not only at the beginning, but also when the fields change values from the field acting on the A block to the field acting on the B block, which occurs at $s = f + \Delta s$ (see eq 5). This latter initialization is required because a discontinuity in the derivative occurs at $s = f$ in the MDE. For both types of initialization, we used RQM4.

Pseudo-Time Integration

Although the pseudo-time integration is not the focus of this manuscript, it plays a particularly important role in CL. Here we have written the pseudo-time integration algorithms for CL; however, the SCFT analog can be easily obtained by eliminating the random force term.

One algorithm is a predictor-corrector[16] version of Euler-Maruyama (EM), which we call EMPC. The EMPC scheme can be written as

$$w^p_{\pm,\mathbf{r}} = w^t_{\pm,\mathbf{r}} - \lambda_\pm \Delta t \left(\frac{\delta H[w^t_+, w^t_-]}{\delta w_\pm(\mathbf{r})} \right) + \eta^t_{\pm,\mathbf{r}}, \tag{22}$$

$$w^{t+\Delta t}_{\pm,\mathbf{r}} = w^t_{\pm,\mathbf{r}} - \frac{\lambda_\pm \Delta t}{2} \left(\frac{\delta H[w^t_+, w^t_-]}{\delta w_\pm(\mathbf{r})} + \frac{\delta H[w^p_+, w^p_-]}{\delta w_\pm(\mathbf{r})} \right) + \eta^t_{\pm,\mathbf{r}} \tag{23}$$

where the statistics of $\eta^t_{\pm,\mathbf{r}}$ are

$$\langle \eta^t_{\pm,\mathbf{r}} \rangle = 0, \tag{24}$$

$$\langle \eta^t_{\pm,\mathbf{r}} \eta^{t'}_{\pm,\mathbf{r}'} \rangle = \frac{2\lambda_{\pm}\Delta t M}{V} \delta_{t,t'} \delta_{\mathbf{r},\mathbf{r}'}. \tag{25}$$

The same noise is used for both the corrector and predictor steps; it is then updated for the next time step. Note that to be consistent with Fredrickson, Ganesan and Drolet,[5] we use $\frac{M}{V}\frac{\partial H[w_+,w_-]}{\partial w_\pm}$ as a discretized approximation of $\frac{\delta H[w_+,w_-]}{\delta w_\pm}$ in deriving the statistics of the noise term. For details on this subtle point see Villet.[17]

Another algorithm is an exponential time differencing (ETD) algorithm developed by Villet and Fredrickson[17,18] for CL. Note that we have used the ETD as presented in Villet[17] rather than the predictor-corrector variant of ETD, as presented in Villet and Fredrickson.[18]

$$\hat{w}^{t+\Delta t}_{\pm,\mathbf{k}} = \hat{w}^t_{\pm,\mathbf{k}} - \mathscr{F}\left(\frac{\delta H[w_+,w_-]}{\delta w_\pm(\mathbf{r})}\right)\left(\frac{1-e^{-\lambda_\pm \Delta t A_{\pm,\mathbf{k}}}}{A_{\pm,\mathbf{k}}}\right) + \left(\frac{1-e^{-2\lambda_\pm \Delta t A_{\pm,\mathbf{k}}}}{2\lambda_\pm \Delta t A_{\pm,\mathbf{k}}}\right)^{1/2} \hat{\eta}^t_{\pm,\mathbf{k}} \tag{26}$$

where $\mathscr{F}$ represents a Fourier transform, hats denote Fourier transformed quantities, $A_\pm$ is the coefficient of the stabilizing part of the Fourier transformed linearized force, and $\hat{\eta}^t_{\pm,\mathbf{k}}$ is the Fourier transformed noise with the same real space statistics as for EMPC (see eqs 24 and 25). For the diblock copolymer melt

$$A_{+,\mathbf{k}} = C\hat{g}_D(k^2), \tag{27}$$

$$A_{-,\mathbf{k}} = \frac{2C}{\chi N} \tag{28}$$

where $\hat{g}_D$ is the Debye scattering function for a homopolymer[19] given by

$$\hat{g}_D(k^2) = \frac{2}{k^4}\left(1 - k^2 + \exp(-k^2)\right). \tag{29}$$

k is the magnitude of the wavevector in Fourier space.

Results and Discussion

The three pseudo-spectral algorithms (RK2, RQM4 and CGF4) are compared for both SCFT simulations and CL. For completeness, the algorithms are tested with both static fields and full simulations, and timing data is presented. For static fields, timing data was collected on a 2.66 GHz Intel Xeon x7460 processor using a single core, and for full simulations, timing data was gathered using a nvidia Tesla M2050 GPU and a 2.67 GHz Intel Xeon x5650 core. As GPUs are increasing being used for computational problems including polymer physics,[20–22] this timing data should be especially pertinent. However, we should emphasize that the timing data is dependent on not only the computer architecture and algorithms but also on the specific implementation of the code. Nonetheless, the trends from the timing data should still be highly relevant.

SCFT

We first verify the expected order for each of the three schemes. We ran SCFT simulations of a diblock copolymer with $f = 0.4$ and $\chi N = 14.4$ for a variety of spatial resolutions and a contour resolution of $\Delta s = 1/100$ in a cubic box with a side length of 8.82 R_g, corresponding to a stress-free SCFT configuration; such a melt forms a bicontinuous gyroid structure. The final field configurations were then used as input for the calculation of $q(\mathbf{r}, s)$ and, ultimately, Q (eq 4) at a variety of contour resolutions. The error in Q as a function of the number of contour points ($1/\Delta s$) is shown in Figure 1a. The results are only shown for L = 64 where L is the number of plane waves in a single spatial direction (L = $M^{1/3}$), since the results for different spatial resolutions were qualitatively the same. All three algorithms exhibit the expected error scaling with contour resolution, and RQM4 has a smaller error coefficient than CGF4 meaning that fewer contour points, and thus less memory, is required to reach a given numerical error.

Using these same runs, we computed the run time as a function of the error in Q. These calculations are useful because they decouple the pseudo-time stepping algorithms and the pseudo-spectral algorithms allowing the pseudo-spectral algorithms to be tested independently. Addition-

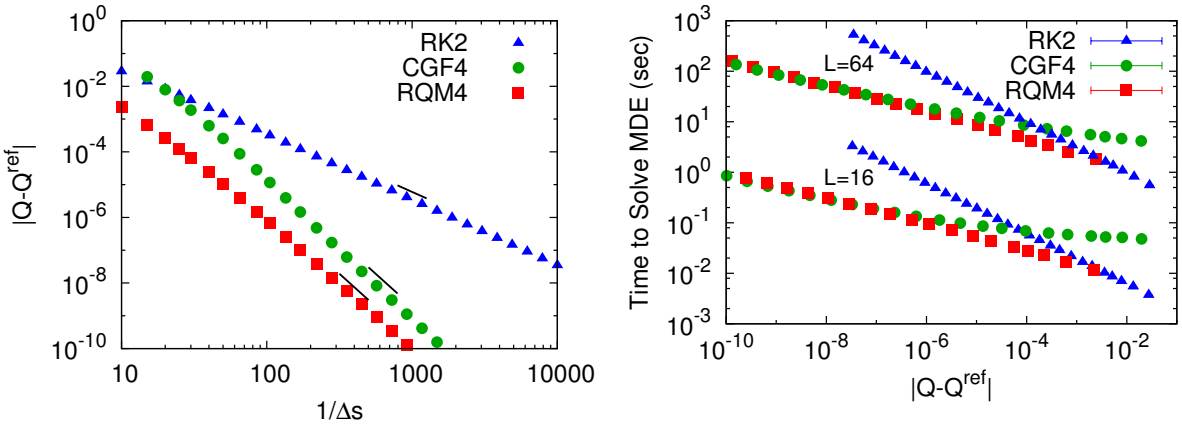

(a) (b)

Figure 1: Performance of the three pseudo-spectral algorithms for static fields generated using SCFT. (a) Error in Q versus contour points ($1/\Delta s$) for L = 64. Black lines denote the expected scalings for each method. (b) Time to solve MDE versus error in Q. Q^{ref} is taken to be Q calculated using RQM4 with $\Delta s = 1/20,000$.

ally, they form a reference for the timing data for full SCFT simulations. These results are shown in Figure 1b. For a given error in Q, the most efficient algorithm is the one that takes the least computational time. Using this as a benchmark, we find that RQM4 is the most efficient algorithm for errors in Q larger than 10^{-7}, and RK2 is not competitive with the two fourth-order algorithms considering that the smallest number of contour points plotted for RQM4 is 10. For errors in Q smaller than 10^{-7}, CGF4 becomes competitive with RQM4 and is marginally faster in our implementation. Consequently, depending on the error tolerance required, these results suggest that one of the fourth-order methods would be the most efficient.

Moving beyond timing data for static fields, we calculated the total time required to run a full SCFT simulation from random initial conditions until the ℓ^2-norm of both of the forces (eqs 8 and 9) are less than 10^{-8}. Using the ETD algorithm with $\Delta t = 1$ and $\lambda_+ = \lambda_- = 5$, the resulting data was plotted as a function of the error in the intensive free energy F_V and can be seen in Figure 2a for the same gyroid structure as in Figure 1. Additionally, full SCFT simulations were run for a diblock copolymer with $f = 0.5$ and $\chi N = 18.8$, which forms a lamellar structure (see Figure 2b) and has a stress-free period of 3.98 R_g. For ease of comparison with the results for the gyroid structure, we chose to run the simulations of the lamellar phase in 3D. Note that in Figure 2, the

ℓ^2-norm of the force for some of the runs using CGF4 (denoted by open symbols in Figure 2) fails to reach the prescribed tolerance. In these cases, the ℓ^2-norm reached a plateau value and subsequently did not decrease.

Upon investigation, we found that the saturation of the ℓ^2-norm was due to errors in the average values of the density fields, which should be be conserved quantities in the theory. These errors prevented incompressibility from being satisfied (the average of eq 8) and thus prevented the ℓ^2-norm from reaching its specified tolerance. This error in the average values of the densities comes from errors in the forward (q) and backward ($q^\dagger$) propagators, which are required to compute the densities (see eqs 10 and 11). This can be seen by computing Q from eq 4 and Q from $1/V \int d\mathbf{r}\, q^\dagger(\mathbf{r}, s=1;[w])$. Both ways of calculating Q should produce the same value. However, for CGF4, due to the reinitialization when the fields change values at $s = f + \Delta s$, the two methods produce different values of Q unlike RK2 and RQM4. Indeed, this reinitialization occurring at $s = f + \Delta s$ breaks the symmetry between the MDE for the forward and backward propagators (eqs 1 and 12, respectively) and introduces $\mathscr{O}(\Delta s)^4$ error into the forward and backward propagators and subsequently the force. In our numerical tests we observed that this error decreased with Δs at a rate of 3.5, close to the expected fourth order. For symmetric polymers, the MDEs for the forward and backward propagators are identical and the value for Q is independent of the method used to compute it. Thus, for the special case of symmetric polymers, the average values of the densities will not have additional $\mathscr{O}(\Delta s)^4$ error and the ℓ^2-norm of the force will not saturate. However, for most polymer architectures, we would expect to see the saturation of the ℓ^2-norm when using CGF4.

We define efficiency in terms of the run time for a given error. For the full SCFT simulations, the relevant run time is the full simulation time and the relevant error is that in F_V. Consequently, for the gyroid structure and the chosen contour resolutions RQM4 is the preferred algorithm; even the smallest number of contour points $1/\Delta s = 25$ results in an error in F_V less than 10^{-4}. Although CGF4 and RQM4 exhibited similar efficiencies for static fields and small errors in Q, RQM4 is more efficient for the full SCFT simulations. For lamellae, RQM4 also is normally preferable. In

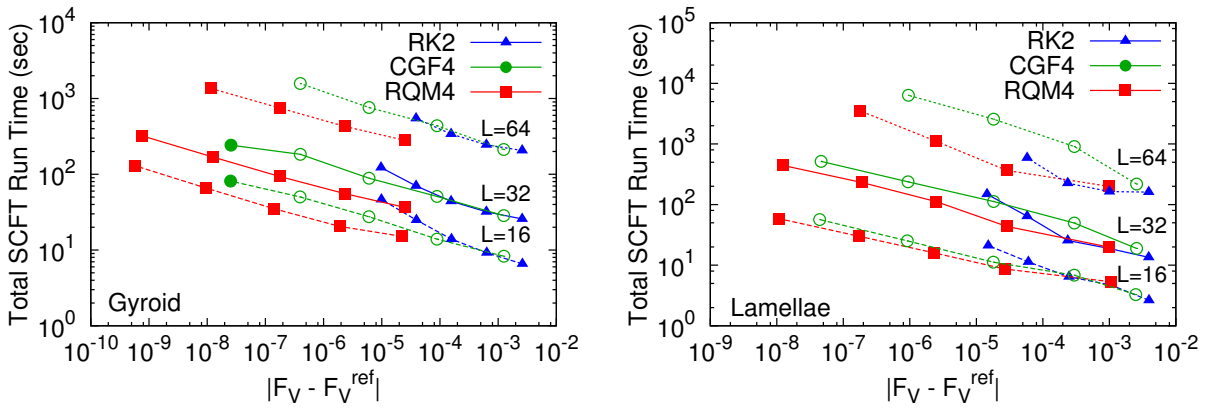

(a) (b)

Figure 2: Total SCFT run time versus error in the intensive free energy for (a) a bicontinuous gyroid structure with $f = 0.4$ and $\chi N = 14.4$ and (b) lamellae with $f = 0.5$ and $\chi N = 18.8$. Long dashed lines, solid lines and short dashed lines correspond to L=16, 32 and 64, respectively. Open symbols denote that the ℓ^2-norm of the force failed to reach the stopping criterion of 10^{-8}. Results are for contour resolutions of $\Delta s = 1/25, 1/50, 1/100, 1/200$ and for L $\neq 64$, $1/400$. The reference intensive free energy was determined from an SCFT simulation using RQM4 and $\Delta s = 1/800$ for the specified spatial resolution with the exception of L=64 for which $\Delta s = 1/400$ was used due to memory constraints on the GPU.

some cases (L=48 and error in $F_V > 10^{-4}$), RK2 is marginally faster for a given error in F_V, but requires more contour points (twice as many at an error in F_V of 10^{-3}) and thus more memory. The overall performance of RQM4 is surprising since it requires an additional two FFT pairs per contour step compared to CGF4, but this is likely due to an improved error coefficient (see Figure 1) and the lack of additional error that prevents ℓ^2-norm of the force from reaching its target in the CGF4 simulations. Overall, these results are in general agreement with those published by Stasiak and Matsen,[14] although they used Anderson mixing rather than ETD to update the field configurations.

Complex Langevin

Unique to this study, we investigated the performance of the three MDE algorithms using CL. These runs were done with the same parameters as in the SCFT case: a diblock copolymer with $f = 0.4$ and $\chi N = 14.4$. Unlike SCFT, where we took the final field configuration, for CL, we ran

a full simulation using the ETD algorithm with $C = 50$, $\Delta s = 1/100$, $\Delta t = 1$ and $\lambda_+ = \lambda_- = 10^{-3}$. After the system equilibrated, we took 6 decorrelated field snapshots and solved the MDE for each of these snapshots for a variety of contour resolutions. The error in Q is then averaged across the 6 calculations and plotted as a function of the number of contour points; the result of which is shown in Figure 3a. These results, unlike SCFT, are highly dependent on L. This L dependence is due to the Langevin noise that scales as $L^{3/2}$ (see eq 25) and causes fields with finer spatial resolution to be driven by stronger noise. Thus, for L=64 where the fields are rough, we found that CGF4 has substantial errors in Q for $\Delta s > 1/300$. Note that *all* 6 fields had large errors. However for sufficiently small Δs, all algorithms have the proper asymptotic order of convergence. RQM4 generally produces smaller errors in Q than CGF4 at the same contour resolution for L=16, but for L=64, RQM4 and CGF4 are similar for errors in $Q < 10^{-2}$. Since the results for L=64 are very different from the results for SCFT, it is likely that the conclusions from SCFT will not be applicable for CL.

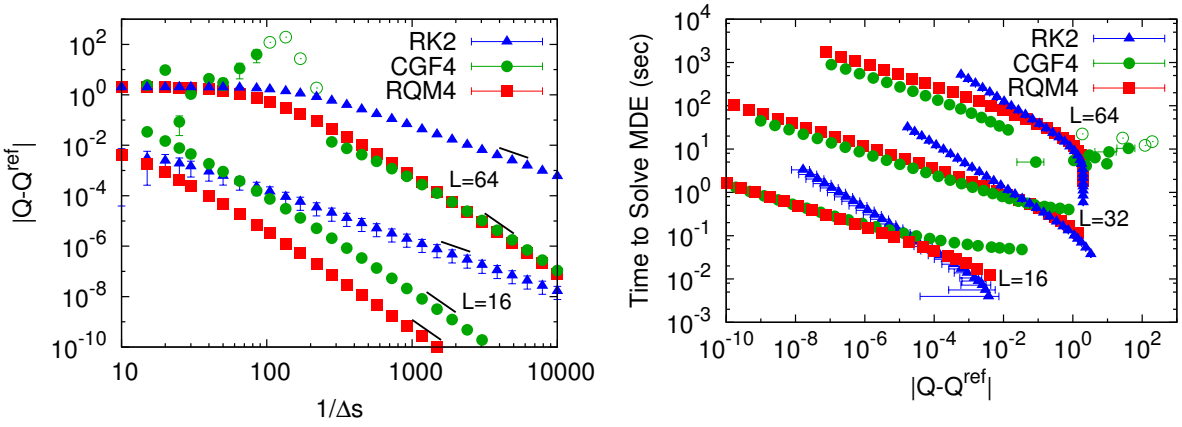

(a) (b)

Figure 3: Performance of the three pseudo-spectral algorithms for static fields generated using CL. (a) Error in Q versus contour points ($1/\Delta s$). Black lines denote the expected scalings for each method. (b) Time to solve the MDE versus error in Q. Open symbols denote points with error bars too large to plot. Q^{ref} is taken to be Q calculated using RQM4 with $\Delta s = 1/20,000$.

We also investigated the time required to solve the MDE as a function of the error in Q for the same runs as in Figure 3a. As can be seen in Figure 3b, these results also vary with L. As with SCFT, the most efficient algorithm is the one that has the shortest run time for a given error in Q.

For both L = 32 and 64 and errors in Q smaller than 10^{-2}, the CGF4 algorithm is the most efficient. For L = 16, both fourth-order methods are competitive for errors in Q less than 10^{-5} and for all L, RK2 is the most efficient for large errors in Q (greater than 10^{-4} for L=16, 10^{-1} for L=32 and 10^{0} for L=64).

Although the timing data in Figure 3b provides some guidance, ultimately, full CL simulations should be used to determine the best pseudo-spectral algorithm. To this end, we ran several CL simulations with different parameters. After equilibration, we calculated the time until the intensive Hamiltonian (H_V) values were decorrelated, which we call the correlation time τ, and determined the run time to τ. This was then plotted as a function of the difference between the average value of the intensive Hamiltonian $\langle H_V \rangle$ and the average value of a reference intensive Hamiltonian, run with the same parameters only using RQM4 and $\Delta s = 1/800$. Since all of the simulations were given the same random number seed, the trajectories from the simulation of interest and the reference simulation are correlated. Thus, to determine the error bars, we used a paired t confidence interval[23] using 95% confidence. For these simulations, we used EMPC with $\Delta t = 1$, $\lambda_+ = 10^{-3}$ and $\lambda_- = 10^{-4}$. These parameters were chosen so that the average value of the Hamiltonian has converged with respect to $\lambda_\pm$ but were not small enough to unnecessarily lengthen the simulation run times. With these parameters, we found that two million time steps provided good statistics.

We considered a variety of contour and spatial resolutions as well as system parameters. However, the largest L considered was L=48 rather than L=64, since at L=64, it was difficult to extract useful data due to the strength of the noise. The results for a gyroid phase with $f = 0.4$, $\chi N = 14.4$ and either $C = 50$ or $C = 150$ can be found in Figure 4, the results for a lamellar phase with $f = 0.5$, $\chi N = 18.8$ and either $C = 50$ or $C = 150$ can be found in Figure 5 and the results for a disordered phase with $f = 0.5$, $\chi N = 10$ and $C = 50$ can be found in Figure 6. All simulation cells were cubic with simulation cell lengths corresponding to an SCFT stress free configurations with the exception of the disordered phase, which was run with a length of $5R_g$. Surprisingly, for all cases except for the gyroid structure with L=16, RK2 is the most efficient algorithm, i.e. it has the shortest run time to τ to reach a given error in $\langle H_V \rangle$. For the gyroid structure with L=16,

the fourth-order methods are likely more efficient because of the smoother fields due to the large spatial resolution $\Delta x = (\text{simulation cell length})/L = 0.55$ as compared to lamellae with $\Delta x = 0.25$ and disordered with $\Delta x = 0.31$ for L=16. Not only is RK2 unusually the most efficient algorithm, it also has shorter run times to τ for a *fixed* Δs, which can be seen by comparing the left most point, which corresponds to $\Delta s = 1/400$ for a L=32 or 64 in Figures 4, 5 and 6. Note that the error bars are larger for RK2 than for RQM4 or CGF4, because RQM4 is used as the reference. In fact, all three methods have similar variances and error of mean for the intensive Hamiltonian at specified Δs.

With regards to the stability of the CL trajectories, we define an unstable trajectory as one in which a field value becomes infinite or not a number regardless of the cause of the instability. With this definition, we find that trajectories using RQM4 were normally stable and most trajectories using RK2 were stable. When trajectories using RK2 did go unstable they were usually at a combination of large L, large Δs or small C. Trajectories using the CGF4 were more likely to go unstable, which could be anticipated from the results with static fields (see Figure 3).

Since the error in Q is less for RQM4 than RK2 given the *same* static field (see Figure 3a) while the error in $\langle H_V \rangle$ is less for RK2 than RQM4 for some parameters, there is clearly an intricate coupling of the diffusion algorithm and the pseudo-time stepping algorithm such that in full CL simulations, RK2 produces smaller errors in $\langle H_V \rangle$. This coupled with the shorter run times to τ for a given Δs for RK2 compared to the fourth-order methods, makes it preferable. This is in direct contrast with SCFT, where RQM4 is generally the preferred algorithm. In an effort to understand why the second-order method is more efficient than the fourth-order methods for the full CL simulations, we consider the role of the schemes for the MDE. During the course of a CL simulation, random noise is introduced in the fields during the pseudo-time integration (eq 14). Then the non-smooth fields are used in the MDE (eq 1). This turns the propagator into an stochastic process itself. Finally, the propagator is used to compute the densities (eqs 10 and 11) and the force (eqs 9 and 8) resulting in a feedback loop. Because q is no longer smooth, the dissipative properties of the MDE scheme become more relevant than the local truncation error

to determine the actual accuracy of the method (see p. 147 and Section 10.4 of Strikwerda[24]). Although the CGF4 scheme has good dissipation,[25] RQM and RK2 have improved dissipation due to the way in which the diffusion operator is handled. Additionally, since RQM4 is obtained from the RK2 by extrapolation, it is expected that the lower order RK2 would be have stronger high modal decay. Therefore, the superior performance of RK2 is very likely due to its improved dissipative properties.

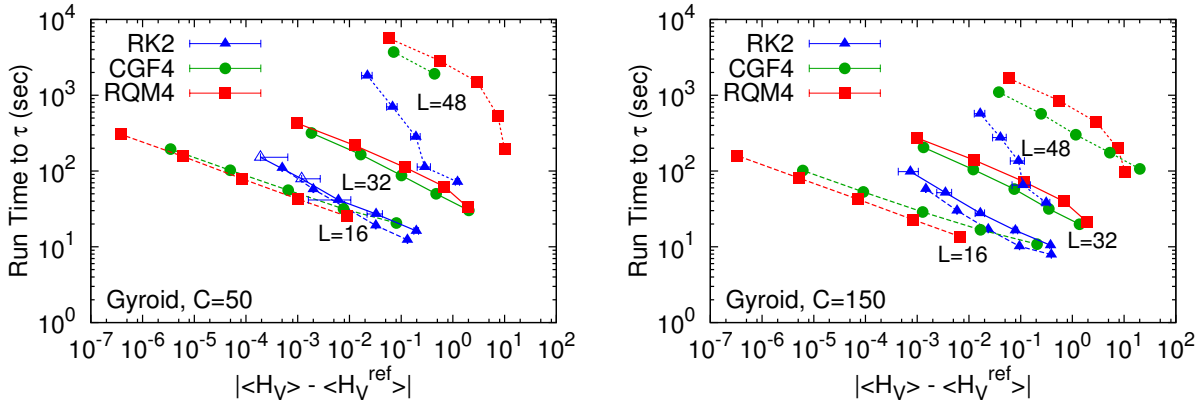

(a) (b)

Figure 4: Run time to τ versus error in the average value of the intensive Hamiltonian for a bicontinuous gyroid structure with $f = 0.4$, $\chi N = 14.4$ and either (a) $C = 50$ or (b) $C = 150$. Long dashed lines, solid lines and short dashed lines correspond to L= 16, 32 and 48, respectively. Open symbols denote that error bar on the left hand side continues to zero. Results are for contour resolutions of $\Delta s = 1/25, 1/50, 1/100, 1/200, 1/400$, and missing points indicate that the simulation went unstable. The reference average Hamiltonian was determined from CL using RQM4 and $\Delta s = 1/800$ for the specified spatial resolution.

However, we also test whether adjusting the time stepping algorithm or the model changes the results. Specifically, we used ETD with the same time step, added compressibility to the model and smeared the mass of the monomers (a regularization technique). To introduce compressibility, the delta functional in the original particle based model ($\delta(\phi_A + \phi_B - 1)$) is replaced with $\exp(-\zeta NC/2 \int d\mathbf{r}\,(\phi_A + \phi_B - 1)^2)$.[26] This results in the addition of $C/(\chi N + 2\zeta N) \int d\mathbf{r}\, w_+^2(\mathbf{r})$ to the Hamiltonian (eq 3). Here we chose $\zeta N = 1000$. For smearing the mass of the monomers, we adopt the formalism developed by Wang[27] for charged particles and apply it to polymers as done in a recent paper[28] and discussed in length elsewhere.[17] The particle based densities ϕ are replaced

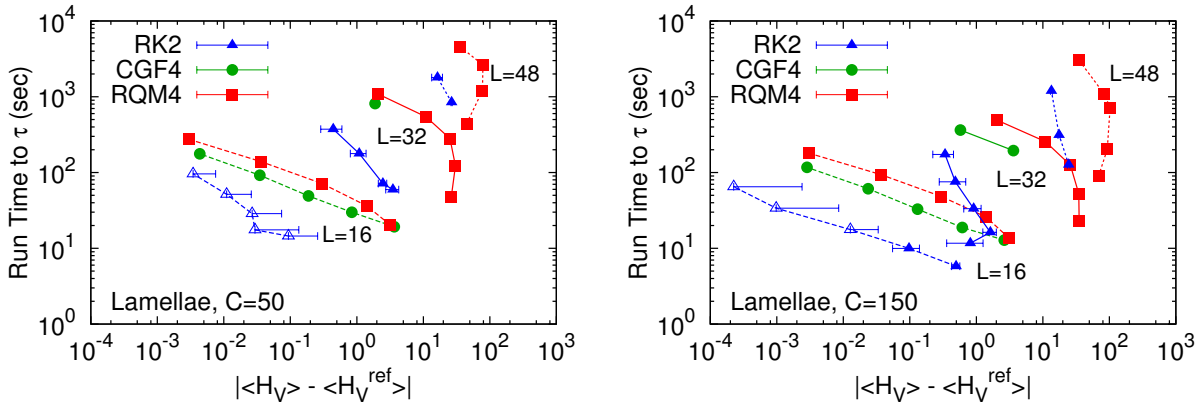

(a) (b)

Figure 5: Same as Figure 4 for a lamellar structure with $f = 0.5$, $\chi N = 18.8$ and either (a) $C = 50$ or (b) $C = 150$.

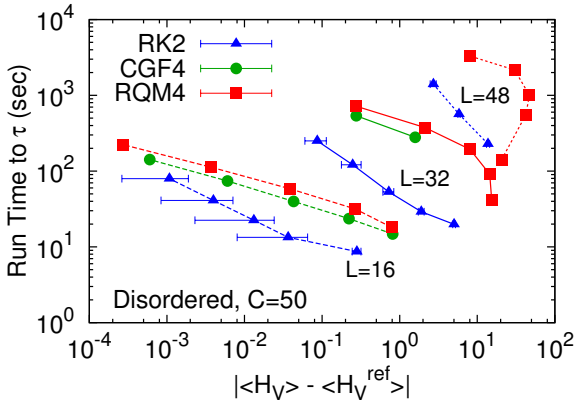

Figure 6: Same as Figure 4 for a disordered structure with $f = 0.5$, $\chi N = 10$ and $C = 50$.

with $\Gamma * \phi$ where $*$ represents a convolution and $\Gamma = (2\pi^2 a^2)^{-3/2} \exp(-|\mathbf{r}|^2/(2a^2))$; also, a compressible model is used. The Hamiltonian for the model with monomer mass smeared is the same as the Hamiltonian for the compressible model only with w in Q replaced by $\Gamma * w$. Although introducing smeared monomer mass creates another length scale a, it removes UV divergences from the theory for physical properties such as the chemical potential, so that they converge to a finite value with increasing spatial resolution.[17] Here, we have chosen $a = 0.15R_g$ so that the physical properties calculated form simulations of the lamellar phase are invariant to spatial resolution for L$\geq$ 32.

Using the lamellar phase with $C = 50$, $f = 0.5$ and $\chi N = 18.8$ as a reference, we collected timing data for these three modifications and plotted it alongside the original data from Figure 5 as can be seen in Figure 7. Both ETD and the compressible model exhibit roughly the same behavior as the original model, although the fourth-order methods have longer run times to τ. For ETD and $\Delta s = 1/400$, all pseudo-spectral methods take more computational time to reach τ as compared to those of EMPC. Nonetheless, RK2 still exhibits the a reduction in run time to τ for a given error in $\langle H_V \rangle$ as compared to the fourth-order methods for fixed spatial and contour resolutions. For the model with smeared monomer mass, the error in the intensive Hamiltonian is significantly smaller than for the other two models. However, the system takes much longer to equilibrate (roughly two million steps) such that longer runs were required to collect good statistics. The correlation times for H_V were longer, too. Even in this case, where the fields are smoother than than the original model due to the convolution in Q, RK2 still is the most efficient algorithm. Consequently, we can conclude that RK2 is normally the best algorithm for CL simulations for the systems we have tested. Given the range of models, pseudo-time stepping algorithms and breadth of simulation parameters, it is also likely that these results are applicable to other systems, models and pseudo-time stepping algorithms.

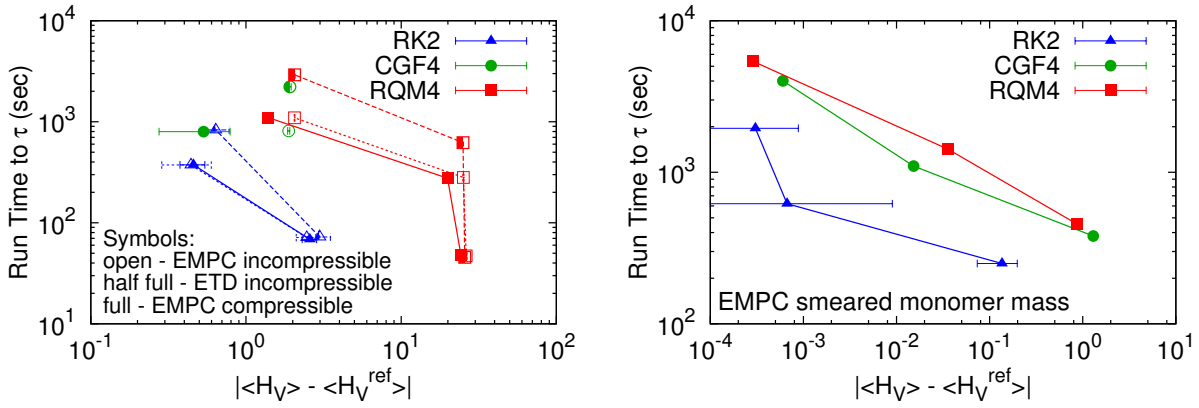

(a) (b)

Figure 7: Run time to τ versus error in the average value of the intensive Hamiltonian for a lamellar structure with $f = 0.5$, $\chi N = 18.8$ and $C = 50$. (a) Runs using the same data as Figure 5a, ETD time stepping algorithm and EMPC time stepping algorithm with a compressible model. (b) Runs using the EMPC time stepping algorithm and a compressible model with smeared monomer mass. Results are for contour resolutions of $\Delta s = 1/25, 1/100, 1/400$, and missing points indicate that the simulation went unstable. The reference average Hamiltonian was determined for CL using RQM4 and $\Delta s = 1/800$ for the specified spatial resolution.

MDE Algorithm Stability

Finally, we discuss the stability of the three MDE schemes for homogeneous fields. For CL, the fields are non-smooth and the magnitudes of the field values can be quite large. Since the Laplacian is treated implicitly in CGF4, the stability constraint is a result of the field values and the explicit treatment of the source term. Since stability is difficult to assess for random fields except by numerical experimentation, we analyzed the stability of each algorithm for the idealized situation of a homopolymer in a perfectly homogeneous field, i.e $w(\mathbf{r}, s) = w$, a constant. Ascher *et al.*[25] analyzed this scheme for discretized version of an advection diffusion equation. For a homogeneous field the MDE can be written as

$$\frac{\partial q(\mathbf{r}, s; [w])}{\partial s} = -wq(\mathbf{r}, s; [w]). \tag{30}$$

Thus, with an initial condition of $q(\mathbf{r}, s = 0; [w]) = 1$,

$$q(\mathbf{r}, s; [w]) = \exp(-ws). \tag{31}$$

To determine the stability region of CGF4 as applied to eq 30, we look at the amplification factor or equivalently at the roots of the characteristic polynomial. Specifically, we conducted a simplified version of a Fourier analysis for multi-step schemes.[24] Since the equation of interest is spatially homogeneous, we are only concerned with the amplification of errors due to the contour stepping. The amplification factor can be determined by substituting q_n with $g^n q_0$ into the CGF4 scheme (eq 21) without the Laplacian term. This, within a multiplicative factor, results in the characteristic polynomial

$$\Phi(g) = \left(\frac{25}{12}\right) g^4 + (-4 + 4w\Delta s)g^3 + (3 - 6w\Delta s)g^2 + \left(-\frac{4}{3} + 4w\Delta s\right) g + \left(\frac{1}{4} - w\Delta s\right). \tag{32}$$

The scheme is stable, i.e. the errors are not amplified without a bound, when each of the j roots of the amplification polynomial, τ_j, satisfy $|\tau_j| \leq 1$ where τ_j is a simple root and $|\tau_j| < 1$ where τ_j is a multiple root. This analysis is only valid for solutions that decay; therefore, the lower bound of the stability region is $\Re(w) > 0$. The resulting stability region for CGF4 is shown in Figure 8. The implication is that for CGF4 with $w = 100i$, which is comparable to maximum field values observed in our full CL simulations with L=48 for a gyroid structure with $C = 50$ and $\chi N = 14.4$, a minimum of 180 contour points are required for stability. This is in agreement with our full CL simulation results; the simulation is unstable for 100 contour points and stable for 200 contour points. Also note that if a rough field is shifted by a sufficiently large constant, CGF4 can develop instabilities. In contrast, both RK2 and RQM4 are always exact and stable for homogeneous fields. This is because both schemes reduce to

$$q_{n+1} = \exp(-w\Delta s)q_n = \exp(-wn\Delta s), \tag{33}$$

which is clearly exact at each contour point. Due to the stochastic nature of CL, it is difficult to know *a priori* what the field intensities will be and therefore the contour resolution that will be required in order to circumvent any instabilities in CGF4. While the above stability analysis is evidently greatly simplified in that it is restricted to homogeneous fields, the qualitative agreement with our numerical simulations for static, rough fields suggests that the analysis has identified the origin of the stability constraints on CGF4.

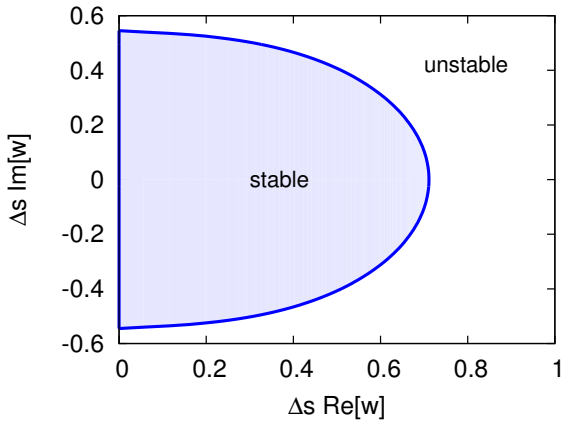

Figure 8: Stability region for CGF4 with a homogeneous field and a uniform initial condition.

Conclusions

We have found that for pseudo-spectral SCFT simulations, the RQM4 method for solving the modified diffusion equation is often the most efficient method for a canonical test system of a diblock copolymer melt; a conclusion which is in agreement with the previous study by Stasiak and Matsen.[14] Additionally, we have found that the reinitialization in CGF4 likely causes error to be introduced into the average values of the densities that can result in a violation of incompressibility and a failure of an SCFT simulation to reach its specified tolerance.

For CL simulations, the RK2 method often achieves a given error in $\langle H_V \rangle$ in shorter run times to a correlation time τ as compared to both CGF4 and RQM4, which is unanticipated from the solution of the MDE with static fields. Nonetheless, this conclusion holds for different microstructures, different spatial resolutions, and different C (Ginzberg, chain overlap) parameters. Ultimately, the

reason for the superior performance of RK2 is linked to the highly non-linear and stochastic nature of coupled system of equations and the strong dissipation of the scheme. Although the crosstalk between the diffusion algorithm and pseudo-time stepping algorithm is present is SCFT, it is much stronger in CL where noise is added to the fields at every time step and the role of dissipation is more important. We also found that RK2 outperforms the fourth-order methods for a different pseudo-time integration algorithm (ETD as opposed to EMPC), a compressible diblock copolymer model, and a compressible diblock copolymer model with monomer mass smeared. Given its consistent performance for these different models and methods, RK2 is evidently the method of choice for a broad range of polymer systems, parameter choices, and pseudo-time stepping algorithms.

Finally, the stability limit of CGF4 for complex, homogeneous fields was computed analytically. We found that the stability region largely mirrored its numerical behavior with the rough fields observed in CL, and thus can be used to choose a proper contour resolution. We also found that in this idealized case both RK2 and RQM4 are unconditionally stable. Ultimately, we expect that our conclusions on not only the stability, but choice of diffusion equation scheme for SCFT and CL can be be extended beyond diblock copolymer melts to field-theoretic simulations of broader classes of self-assembling polymeric fluids.

Acknowledgement

We acknowledge support from the Center for Scientific Computing at the CNSI and MRL: an NSF MRSEC (DMR-1121053) and NSF CNS-0960316. DJA was supported by the Institute for Collaborative Biotechnologies through contract W911NF-09-D-0001 from the U.S. Army Research Office. KTD was supported by the National Science Foundation SOLAR program (CHE-1035292). HDC acknowledges support form NSF grant DMS 1016310. We would also like to thank Dr. Nathaniel Lynd for helpful discussions.

Supporting Information Available

References

(1) Matsen, M. W. *J. of Phys.: Condens. Matter* **2002**, *14*, R21.

(2) Fredrickson, G. H. *The Equilibrium Theory of Inhomogeneous Polymers*; Clarendon Press: Oxford, 2005.

(3) Matsen, M. W. In *Soft Matter, Volume 1: Polymer Melts and Mixtures*; Gompper, G., Schick, M., Eds.; Wiley-VCH: Weinheim, 2006.

(4) Ganesan, V.; Fredrickson, G. H. *Europhys. Lett.* **2001**, *55*, 814–820.

(5) Fredrickson, G. H.; Ganesan, V.; Drolet, F. *Macromolecules* **2002**, *35*, 16–39.

(6) Matsen, M. W.; Schick, M. *Phys. Rev. Lett.* **1994**, *72*, 2660–2663.

(7) Rasmussen, K. Ø.; Kalosakas, G. *J. Polym. Sci., Part B: Polym. Phys.* **2002**, *40*, 1777–1783.

(8) Tzeremes, G.; Rasmussen, K. Ø.; Lookman, T.; Saxena, A. *Phys. Rev. E* **2002**, *65*, 041806.

(9) Strang, G. *SIAM Journal on Numerical Analysis* **1968**, *5*, 506–517.

(10) Ranjan, A.; Qin, J.; Morse, D. C. *Macromolecules* **2008**, *41*, 942–954.

(11) Cochran, E. W.; García-Cervera, C. J.; Fredrickson, G. H. *Macromolecules* **2006**, *39*, 2449–2451.

(12) Cochran, E. W.; García-Cervera, C. J.; Fredrickson, G. H. *Macromolecules* **2006**, *39*, 4264–4264.

(13) Hur, S.-M.; Garcí-Cervera, C. J.; Fredrickson, G. H. *Macromolecules* **2012**, *45*, 2905–2919.

(14) Stasiak, P.; Matsen, M. *Eur. Phys. J. E: Soft Matter Biol. Phys.* **2011**, *34*, 1–9.

(15) Lennon, E. M.; Katsov, K.; Fredrickson, G. H. *Phys. Rev. Lett.* **2008**, *101*, 138302.

(16) Öttinger, H. C. *Stochastic Processes in Polymeric Fluids*; Springer: Berlin, 1996.

(17) Villet, M. C. Advanced Computational Field Theory Methods for Fluctuating Polymer Solutions. Ph.D. thesis, University of California, Santa Barbara, 2012.

(18) Villet, M. C.; Fredrickson, G. H. *The Journal of Chemical Physics* **2010**, *132*, 034109.

(19) de Gennes, P.-G. *Scaling Concepts in Polymer Physics*; Cornell University Press: Ithaca, NY, 1979.

(20) Wright, I.; Wickham, R. A. *Journal of Physics: Conference Series* **2010**, *256*, 012008.

(21) Gao, J.; Song, W.; Tang, P.; Yang, Y. *Soft Matter* **2011**, *7*, 5208–5216.

(22) Delaney, K. T.; Fredrickson, G. H. *Computer Physics Communications* **2013**, *184*, 2102 – 2110.

(23) Devore, J. L. *Probability and Statistics for Engineering and the Sciences*, 6th ed.; Brooks/Cole—Thomson Learning: Belmont, CA, 2004.

(24) Strikwerda, J. C. *Finite Difference Schemes and Partial Differential Equations*, 2nd ed.; SIAM: Philadelphia, 2004.

(25) Ascher, U.; Ruuth, S.; Wetton, B. *SIAM Journal on Numerical Analysis* **1995**, *32*, 797–823.

(26) Helfand, E. *The Journal of Chemical Physics* **1975**, *62*, 999–1005.

(27) Wang, Z.-G. *Phys. Rev. E* **2010**, *81*, 021501.

(28) Riggleman, R. A.; Kumar, R.; Fredrickson, G. H. *The Journal of Chemical Physics* **2012**, *136*, 024903.

Table of Contents graphic for manuscript entitled "Comparison of Pseudo-Spectral Algorithms for Field-Theoretic Simulations of Polymers". The authors associated with this manuscript are Debra J. Audus, Kris T. Delaney, Hector D. Ceniceros, and Glenn H. Fredrickson.

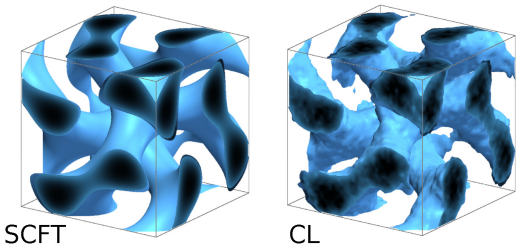

This material is available free of charge via the Internet at `http://pubs.acs.org/`.